Kinematics of the Pacific Equatorial Undercurrent: An Eulerian and Lagrangian Approach from GCM Results

BRUNO BLANKE AND STÉPHANE RAYNAUD

Laboratoire d'Océanographie Dynamique et de Climatologie, Centre National de la Recherche Scientifique, Paris, France

(Manuscript received 26 January 1996, in final form 18 October 1996)

ABSTRACT

Three-dimensional monthly velocity fields from an ocean general circulation model are used to study the annual mean mass balance of the Pacific Equatorial Undercurrent (EUC). Eulerian diagnostics are used to evaluate the various meridional, vertical, and zonal mass fluxes related to the EUC. There are several distinct regimes along the equator, showing clear asymmetries between the western and eastern parts of the basin, and between the northern and southern edges of the EUC. Meridional fluxes are decomposed into pure Ekman divergence and geostrophic convergence, and it is shown that the asymmetries are mainly related to the spatial structure of the Ekman divergence, and thus to that of the trade winds. Lagrangian calculations are used to evaluate accurately the mass transfers between various sections of the EUC and between the EUC domain and the Tropics. The authors show that geostrophic convergence only ventilates the upper layers of the EUC and that the EUC really is a tongue of water flowing from the western Pacific to the Galapagos Islands and beyond. Finally, Lagrangian integrations extended to extratropical regions show that the EUC contributes to an exchange of water between the southern and northern Pacific (and the Indian Ocean through the Indonesian Throughflow): The equatorial zonal pressure gradient draws water from the western boundary currents that originate mostly in the south subtropical gyre. The poleward Ekman divergence associated with the equatorial upwelling distributes EUC water over the surface, with significant recirculation within the EUC (more than 15% of the total transport at 150°W).

1. Introduction

The Equatorial Undercurrent (EUC) is an essential component of the tropical Pacific Ocean circulation. Centered on the equator, it flows eastward as a narrow tongue (roughly 500 km wide) within the equatorial thermocline from north of New Guinea to the Galapagos Islands in the eastern Pacific. It is characterized by a high-salinity core and a high concentration of dissolved oxygen (Tsuchiya 1981). Though the value of its mean transport is still imprecise (due to a lack of direct continuous measurements over its entirety), results inferred from hydrographic or modeling studies estimate 30–40 Sv (Sv $\equiv 10^6$ m^3 s^{-1}). Instantaneous peaks of over 80 Sv have been calculated with geostrophic velocities obtained from expendable bathythermograph temperature and conductivity–temperature–depth data (Picaut and Tournier 1991) and from conductivity–temperature–depth and acoustic Doppler current profiler data in the central Pacific (Chiswell et al. 1995).

Links between the EUC and the extra-equatorial regions were first inferred from the analysis of hydrographic datasets (Lukas 1986; Tsuchiya et al. 1989). The role of the EUC in the basinwide Pacific Ocean circulation and its contribution to the water exchange between tropical and subtropical regions, and between the Northern and Southern Hemispheres, have been addressed more recently using numerical models ranging in complexity from two-layer systems to general circulation models (GCMs) (Pedlosky 1987, 1991; McCreary and Lu 1994; Liu 1994; Liu et al. 1994; Lu and McCreary 1995).

Oceanic GCMs provide a convenient means to study the three-dimensional circulation of a basin such as the tropical Pacific Ocean because they offer a comprehensive and consistent description of the dynamics and thermodynamics. Several studies have already investigated EUC dynamics using GCM simulations (Wacongne 1989, 1990; Blanke and Delecluse 1993). Increased computing resources and progress in parameterizing subgrid-scale phenomena have resulted in more realistic simulations of the tropical ocean circulation, such as those obtained using the Laboratoire d'Océanographie Dynamique et de Climatologie (LODYC) ocean GCM (Blanke and Delecluse 1993; Delecluse et al. 1994; Boulanger et al. 1996; Maes et al. 1997).

In this paper we study the annual-mean structure of the Pacific EUC from a numerical simulation of the climatological annual cycle of the whole tropical ocean

Corresponding author address: Dr. Bruno Blanke, Laboratoire de Physique des Océans, UFR Sciences et Techniques, 6 avenue Le Gorgeu, BP 809, 29285 Brest, Cedex, France.
E-mail: blanke@univ-brest.fr

circulation. We use the LODYC model, referred to here as OPA, to provide a complete three-dimensional description of the velocity field in the Pacific Ocean. Though some analyses are directly derived from a Eulerian description of the circulation, the most exciting results are obtained with a Lagrangian interpretation, involving computation of three-dimensional trajectories within the flow. Section 2 describes the numerical experiment. Section 3 presents diagnostics of various transports associated with the EUC on an annual mean and contrasts various regimes with longitude. A specific insight into geostrophic convergence helps us characterize possible EUC sources. Section 4 uses Lagrangian computations to investigate the mass balance of the EUC. Similar computations are used in section 5 to depict and quantify the extra-equatorial origin and fate of EUC water. Results are summarized in section 6, and details about the Lagrangian method are given in the appendix.

2. The ocean model

A thorough description of the OPA model can be found in its reference manual (Delecluse et al. 1993). The Navier–Stokes equations (with classical additional assumptions) are discretized using finite differences on a staggered ''C'' grid (Arakawa 1972). It enables an easy computation of the three-dimensional velocity streamfunction (see the appendix for more details). In basinwide tropical experiments, we use the turbulent closure model for the mixed layer physics as described by Blanke and Delecluse (1993).

The domain for the simulation covers the whole tropical belt from 47°N and the Southern Ocean to 65°S. The zonal resolution is as high as 0.33° near the western boundaries and is about 0.75° in the middle of ocean basins. The meridional resolution is also variable, being 0.33° at the equator and increasing to 1.5° poleward of 47°N and S. There are 30 levels in the vertical, with the highest resolution (10 m) in the top 150 m. The bottom topography and the coastlines are derived from the $5' \times 5'$ ETOPO5 dataset, which provides an accurate representation of the Indo–Pacific region and the Galapagos Archipelago.

The model is forced by Hellerman and Rosenstein's (1983) wind stress climatology and Esbensen and Kushnir's (1981) heat flux climatology, and the freshwater budget is prescribed as a relaxation toward the Levitus (1982) seasonal surface salinity. Our analyses are carried out over the last year of the 10-year experiment, by which time the upper tropical ocean has adjusted to climatological equilibrium.

3. Eulerian description

We define the EUC to be the eastward flow in the latitude band from 3.55°S to 3.55°N and depth range from −495 m to the surface. These boundaries conveniently eliminate waters from the North Equatorial Countercurrent and the deeper Equatorial Intermediate Current. Our study deals with the structure of the EUC body within 150°E–90°W, where on an annual mean its core is centered on the equator. The behavior of the EUC west of 150°E and east of 90°W is also investigated, but more in connection with the basinwide circulation, when studying the origin and fate of the EUC.

a. Zonal transport

Comparisons of GCM results with other published estimates can be uncertain because of strong interannual variability associated with the tropical ocean dynamics (see Firing et al. 1983; Delcroix et al. 1992). Heterogeneous criteria used to identify the EUC may obscure the comparisons too. Results from our GCM show a pronounced seasonal variability for the EUC zonal transport (Fig. 1). At 170°E, where it is maximum, the model gives 75 Sv in June, whereas the transport drops to 24 Sv in January. Farther eastward, near 160°W, a comparison of the model results with the observational study of Picaut and Tournier (1991) for the period 1979–85 indicates a fair agreement for both the phase and amplitude of the seasonal cycle.

b. Meridional and vertical transports

Figure 2 gives a first diagnostic of possible mass sources and sinks for the EUC. We compute annual mean, meridional and vertical, inflow and outflow transports over 30° wide subregions of the whole box (3.55°S–3.55°N, 150°E–90°W; −495 m–0 m). The associated annual mean EUC transport is also drawn with thick arrows on the equator. The westward transport of the South Equatorial Current (SEC) is not shown on this diagram, but it can be inferred as the residual of all other fluxes. A clear asymmetry exists between the western and eastern Pacific: northward outflows dominate in the west and central Pacific, while southward outflows are dominant in the east. Equatorward inflow occurs primarily in the central Pacific.

We are able to differentiate several regimes. The first one, west of the date line, presents an intense EUC with no loss of flow, associated with a large northward outflow and a small northward inflow (here the net mass balance is provided by a westward decrease in the SEC transport). The situation from the date line to 150°W resembles the first one, but with an increased northward inflow, and the appearance of weak southward inflows and outflows (and almost no modification of the overlying westward transport). Next, from 150°W to 120°W, the northward inflow decreases as well as the EUC flow (and the SEC intensifies to a lesser extent). A fourth regime is found between 120°W and 90°W: the northward outflow is now small and is replaced by an intense southward outflow together with a drastic decrease in the EUC flow.

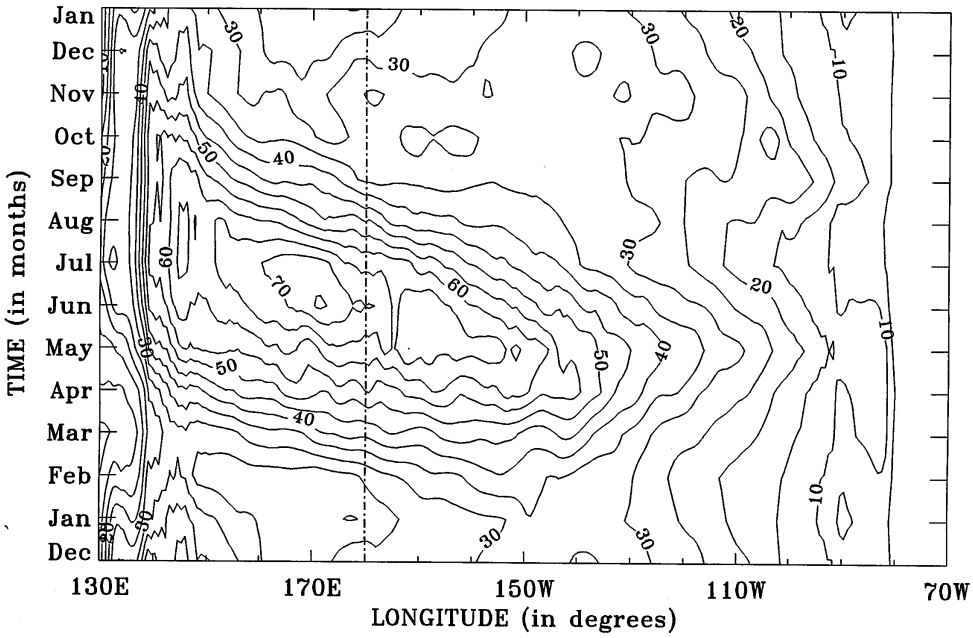

FIG. 1. Time–longitude diagram of the monthly mean EUC transport. The contour interval is 5 Sv.

c. Ekman and geostrophic transports

Our previous mass budgets inform us about the basic circulation in the first 500 m of the equatorial Pacific, but they do not distinguish Ekman divergence and geostrophic convergence, and do not indicate whether strong inflows and outflows are associated with an intense mass exchange with the EUC, or with the SEC.

We compute the Ekman transport directly from the wind stress that forces the GCM,

$$V_{\text{Ekman}}(y) = -\frac{1}{\rho_0 f(y)} \int_{x_0}^{x_1} \tau_x(x, y)\, dx, \qquad (3.1)$$

where f is the Coriolis parameter (computed at y = 3.55°S or 3.55°N), ρ_0 is equal to 1023 kg m^{-3}, τ_x is the zonal wind stress, and x_0 and x_1 represent the bounds of the domain over which the transport is calculated. The vertical turbulent flux is assumed to vanish at z_0 = 495 m, the bottom of our box.

The geostrophic convergence is calculated using two methods. The first method determines the geostrophic transport directly from the zonal pressure gradient computed by the GCM, yielding

$$V^a_{\text{geos}}(y) = \frac{1}{\rho_0 f(y)} \int_{x_0}^{x_1} \int_{-z_0}^{0} \frac{\partial P(x, y)}{\partial x}\, dz\, dx. \qquad (3.2a)$$

The second method approximates it as the difference between the total meridional mass flux and the Ekman transport,

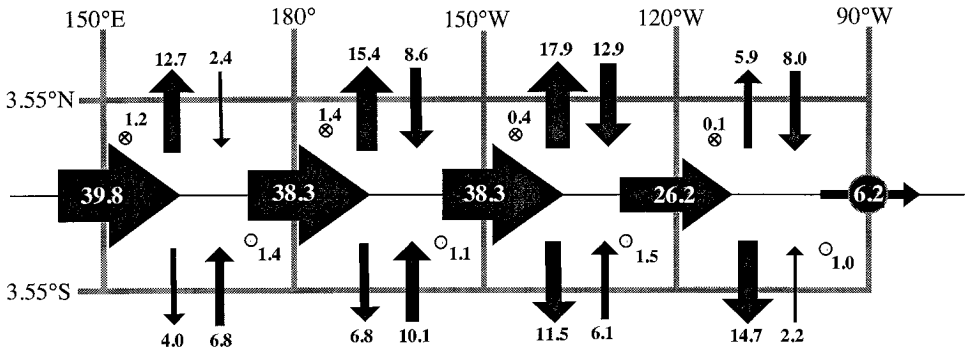

FIG. 2. Meridional and vertical mass exchanges associated with the EUC over four 30° wide subregions. Meridional fluxes (evaluated at 3.55°S and 3.55°N) and vertical fluxes (evaluated at depth −495 m) refer to inflows and outflows as directly deduced from GCM results. The EUC transport (values in white) is also drawn on the equator. The thickness of the arrows is proportional to the horizontal transport they represent. Within each subregion, the mass budget may be nonzero and is related to variations in the transport of the eastward flow (SEC).

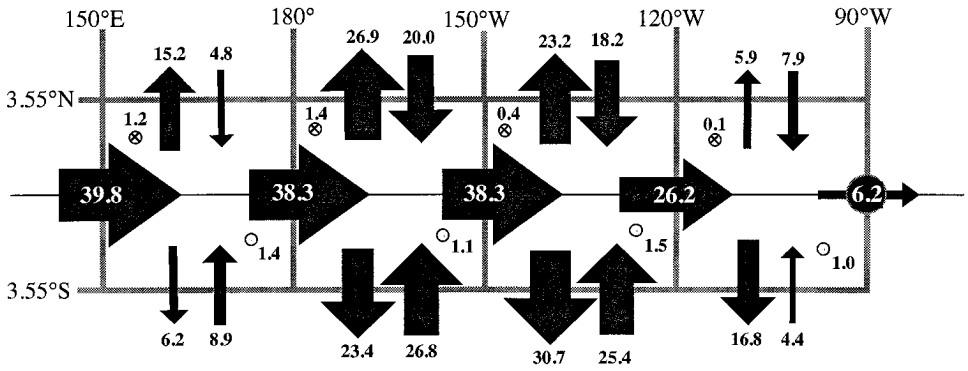

FIG. 3. As in Fig. 2 except that meridional inflows and outflows now refer to geostrophic convergence and Ekman divergence, respectively.

$$V^{b}_{\text{geos}}(y) = V_{\text{total}}(y) - V_{\text{Ekman}}(y). \qquad (3.2b)$$

Both calculations for geostrophic convergence are made at 3.55°S and 3.55°N. There is a good agreement between both methods (not shown), which means that meridional movements near the equator are essentially driven by the zonal wind (poleward Ekman drift induced by the zonal wind stress) and by equatorward geostrophic convergence (due to the basinwide zonal pressure gradient). Diffusive or nonlinear effects do not affect significantly this balance.

Figure 3 shows a modified transport budget for the EUC, with meridional inflows and outflows replaced by Ekman and geostrophic transports. This decomposition explains some asymmetries found in the EUC mass balance. Meridional asymmetries in the zonal wind stress explain the preferential southward outflow of EUC water in the eastern Pacific. Geostrophic convergence is maximum in the central Pacific (with 20.0 Sv entering the EUC basin between 180° and 150°W from the north, and 26.8 Sv from the south) but is partially compensated by Ekman divergence of the same order. Consequently, the net equatorward influx falls to 8.6 Sv at 3.55°N and 10.1 Sv at 3.55°S.

4. Lagrangian description

Our Lagrangian diagnostics are based on an algorithm we developed at LODYC to compute trajectories in a three-dimensional velocity field. This algorithm calculates true trajectories for a given stationary velocity field. In our GCM, the divergence is discretized on a ''C'' grid and allows the exact calculation of three-dimensional streamlines within each box of the three-dimensional mesh (see the appendix). For a stationary field, such streamlines define exact trajectories of particles in the model. This method was applied first to the study of the three-dimensional circulation in the tropical Atlantic, and then to the study of the origin and fate of the waters found in the Strait of Gibraltar (Speich 1992). The technique is extended to time-dependent velocity fields (like monthly outputs) by assuming the velocity is constant over successive periods less or equal to the available sampling.

a. Annual mean velocity field

To assess the relevance of the Lagrangian method and to provide an easy comparison with our first Eulerian diagnostics, computations are done first for the annual-mean velocity field. We study the EUC in the central basin, where its transport and geostrophic convergence are maximum. We introduce particles into the EUC at 180° and 150°W. For both longitudes, the EUC transport inferred from the annual mean zonal velocity is 38.3 Sv. Particles are integrated forward in time from 180° and backward from 150°W. As in the previous section we define a box, including the EUC, bounded by latitudes 3.55°S and 3.55°N, and by the depth −495 m. Exit positions for particles launched at 180° are then located either at depth −495 m, on the northern or southern side of the box, on the meridional section at 150°W, or on the very same section at 180°. Conversely, particles launched at 150°W are tracked backward till they cross the boundaries of the box, either at its bottom (−495 m), its zonal sides (180° or 150°W) or its meridional sides (3.55°S or 3.55°N).

Figure 4 illustrates the results obtained with a homogeneous distribution of particles over both initial sections (one particle every sixth degree × 15 m, namely, 853 particles at 180° and 673 at 150°W). Five different symbols are used on both initial sections (top left and bottom right panels) to represent all possible exit locations: ''plus'' for 3.55°N, ''cross'' for 3.55°S, ''triangle'' for depth −495 m, ''star'' for particles traveling across the whole box 180°–150°W and ''square'' for particles coming back to their initial section. Final positions after zonal crossing of the whole box are also given (top right and bottom left panels) to emphasize the EUC tube-structure.

We quantify mass exchanges between both EUC sections and every side of the box in Fig. 5. These estimates are based on a heterogeneous distribution of the initial

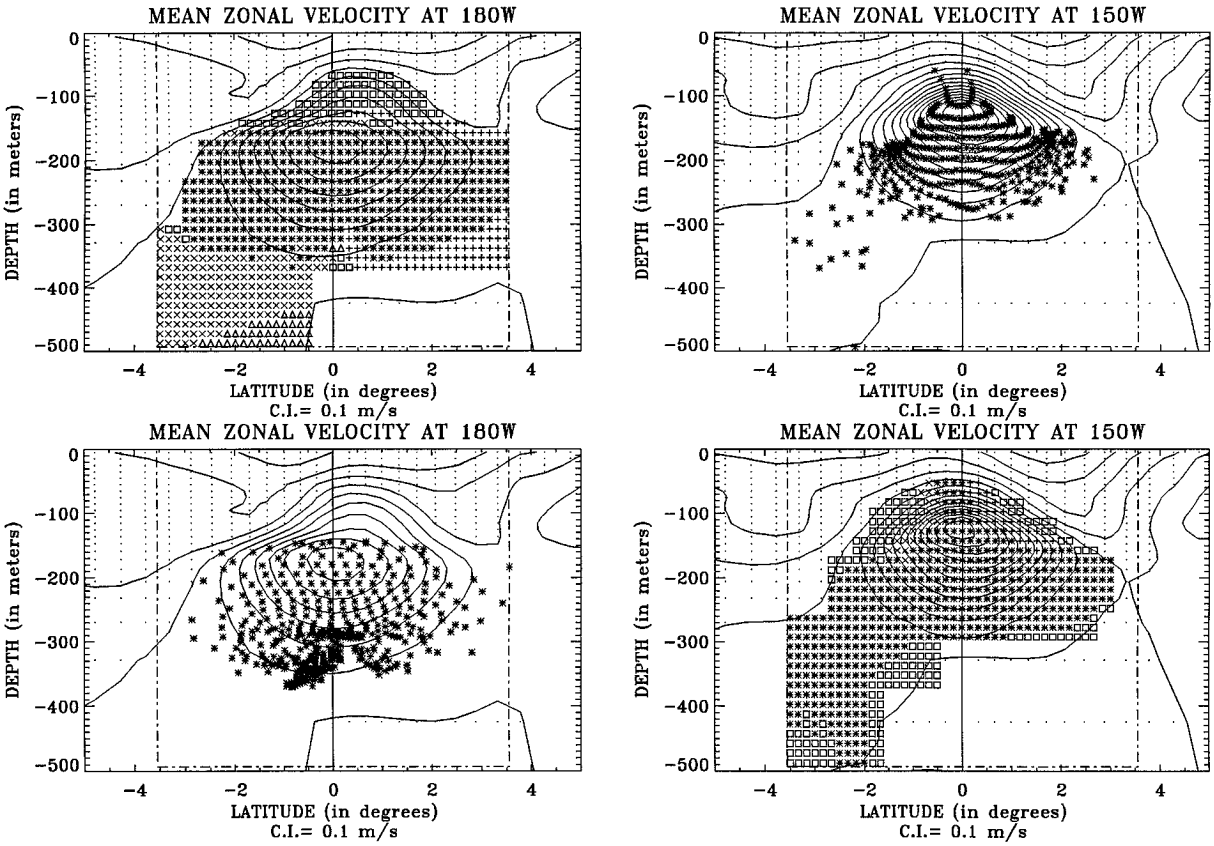

FIG. 4. Example of homogeneous initial distribution of particles at 180° (top left panel) and 150°W (bottom right panel). Five symbols differentiate five possible destinations for the particles: ''plus'' for 3.55°N, ''cross'' for 3.55°S, ''triangle'' for depth −495 m, ''star'' for particles traveling across the whole box 180°–150°W, and ''square'' for particles coming back to their initial EUC section. Integrations are performed forward in time from 180° and backward in time from 150°W, with the annual-mean value of the velocity field. Exact locations of particles traveling across the whole box are given on the associated exit section (top right and bottom left panels).

positions to improve their accuracy (see the appendix for details): 2941 and 2899 particles (each of them associated with less than $T_0 = 0.017$ Sv) are launched over both initial sections, that is, 180° and 150°W respectively. One can verify first that the mass transfer at depth −495 m is almost zero (0.3 Sv): the EUC is insulated from the deeper oceanic layers because the equatorial upwelling does not affect waters below the thermocline. The mass that crosses the entire length of the box, that is, the intensity of the EUC tube, is 30.0 Sv when computed eastward (forward integration) and 29.9 Sv when diagnosed westward (backward integra-

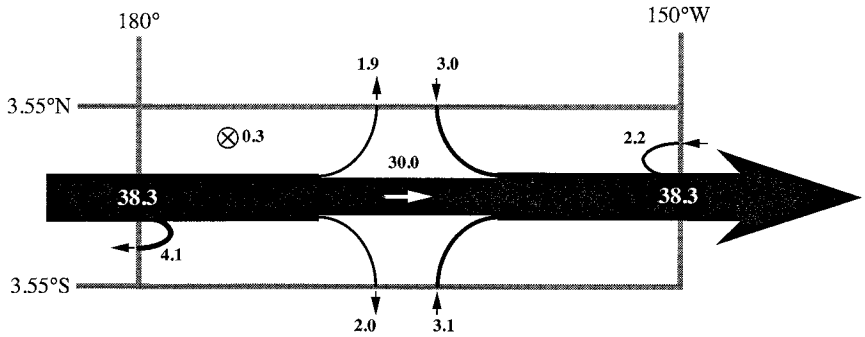

FIG. 5. Quantitative estimates of the various mass exchanges between both EUC sections of box 180°–150°W and the exterior region, as depicted in Fig. 4 (see text for details). White values denote the EUC transport at both longitudes. All transports are in Sverdrups. The thickness of the lines is proportional to the horizontal transport they represent.

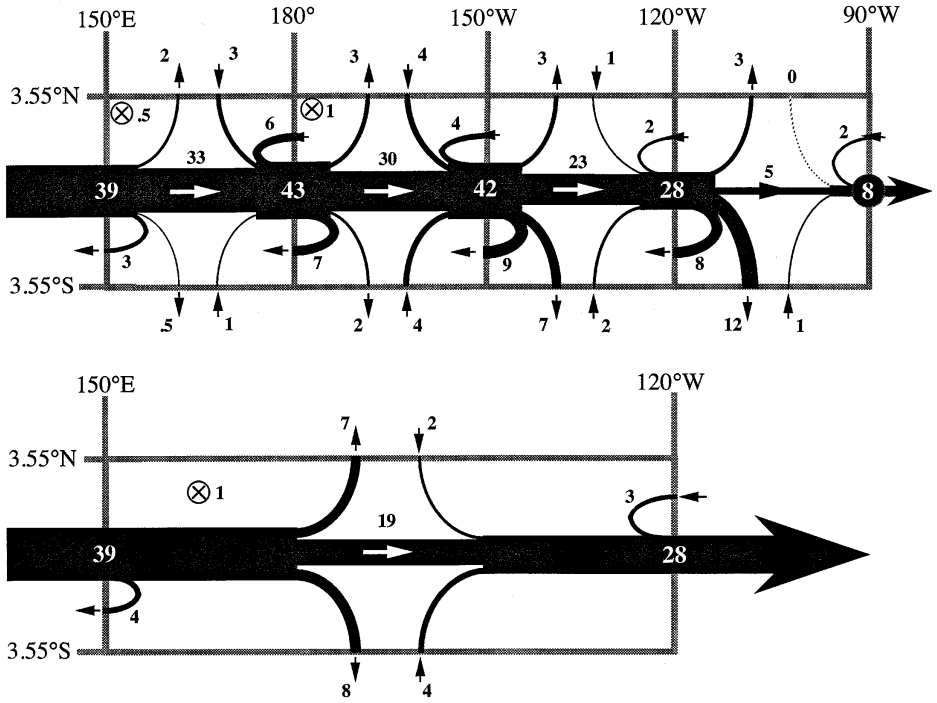

FIG. 6. Same as in Fig. 5 but using the monthly varying velocity field for backward and forward integrations. (a) Results over four 30° wide adjacent subregions. (b) Results for the whole 150°E–120°W region.

tion). The excellent agreement between both values shows the accuracy of the Lagrangian method to diagnose transports.

Less than 22% of the EUC transport at 150°W results from meridional convergence between 180° and 150°W, that is, from 3.55°S (3.1 Sv), 3.55°N (3.0 Sv), and from 150°W SEC water (2.2 Sv). These latter particles enter the box westward (at 150°W) within the SEC at depth range approximately from 100 to 300 m. They converge equatorward within the box and are captured by the EUC before they reach 180°. They leave the box at 150°W in the upper part of the EUC and mostly on its periphery (see Fig. 4). At deeper levels, the EUC flows within or below the thermocline, where the zonal pressure gradient (and thus geostrophic convergence) is negligible.

We compare the 6.1 Sv meridional geostrophic convergence (3.1 Sv at 3.55°S and 3.0 Sv at 3.55°N) that increases the EUC flow between 180° and 150°W with our previous estimate of the total geostrophic convergence integrated from −495 m to the surface and from 180° to 150°W, that is, 26.8 Sv at 3.55°S and 20.0 Sv at 3.55°N (see Fig. 3). Only 13% of the total possible convergence (15% at 3.55°N and 12% at 3.55°S) is actually used to supply the EUC with water in this band of longitude. In terms of fraction of the actual equatorward fluxes (shown in Fig. 2), we find that 33% of the meridionally incoming mass reaches the EUC. The other 12.6 Sv are injected in the surface layers to join the westward flowing SEC. Moreover, the particles that are captured by the EUC are likely to leave it soon because they are rapidly upwelled and distributed in the SEC. This is apparent in the final destination of the top layers of the EUC at 180° (see Fig. 4): most of the particles (at depths shallower than 140 m) do not reach longitude 150°W but leave the box by the initial section (4.1 Sv), or by the meridional boundaries (2.0 Sv at 3.55°S and 1.9 Sv at 3.55°N). As the box 180°–150°W is chosen at the location of maximum geostrophic convergence, we conclude as Lu and McCreary (1995) that such a mechanism plays a minor role along the EUC, ventilating the upper structure only. Deeper particles of the EUC are not affected by convergence phenomena and can be tracked within the core of the EUC back to the western part of the basin, or followed to the eastern Pacific, as shown in the next subsection.

b. Monthly varying velocity field

Lagrangian integrations are done within all four 30° long boxes (from 150°E to 90°W). We still focus on annual-mean results but, to obtain more realistic estimates, we use hereafter the monthly varying velocity field to compute trajectories: initial positions are diagnosed for all 12 months and integrations now account for seasonal variability. Annual-mean mass exchanges between the EUC and zonal, meridional, and vertical sides of the boxes are given in Fig. 6a. They are defined

as the arithmetic mean of 12 independent monthly Lagrangian experiments.

The results for the box 180°–150°W compare well with the transports obtained with the annual-mean velocity field (see Fig. 5). Accounting for seasonal variability slightly modifies the value of annual-mean mass exchanges, but differences occur primarily in the EUC transport computed at 180° and 150°W. Transports deduced from the 12-month average of the circulation (38.3 Sv in Fig. 5) are naturally smaller than the 12-month average of the seasonal transport (43 and 42 Sv in Fig. 6a) since zonal velocity may locally change sign throughout the year. This increase of annual-mean EUC transport (by roughly 5 Sv) is associated with increased mass exchanges between the EUC and the meridional limits of the box (by roughly 1 Sv for all transfers) and increased exchanges between the EUC and the SEC within the box (by roughly 2 Sv). The basic structure of the circulation, particularly the tube-structure intensity for the EUC (30 Sv), is however very similar in both cases. This limited and only local impact of the annual cycle agrees with Lu and McCreary's (1995) results, which showed that annually varying winds do not significantly modify the large-scale structure of the meridional cell that carries subtropical water to the equator.

Diagnostics along the equator offer a comprehensive view of the zonal and meridional circulations associated with the EUC and its termination. All over the Pacific Ocean, the EUC loses water through equatorial upwelling and Ekman divergence. West of 150°W this phenomenon is largely balanced by geostrophic convergence that brings shallow water to the equator that mixes downward from the overlying SEC. East of 150°W the EUC core draws nearer the surface, and becomes more affected by Ekman divergence, which is maximum at the surface. The asymmetric meridional structure of the annual-mean wind stress gives more weight to southward exports.

From 150°E to 120°W, the total mass inflow to the EUC by convergence is 27 Sv, that is, the sum of all mass transfers between the EUC and the meridional sides of the 3 associated 30° boxes, and between the EUC and SEC within each 30° box. We diagnose here how much of this convergence actually contributes to the EUC transport at 120°W (28 Sv). For this purpose we track EUC water at 120°W backward in time within a box longer in longitude (150°E–120°W). The results are given in Fig. 6b. We find that 19 out of 23 Sv of EUC water flowing from 150°W to 120°W in fact originate from 150°E, and thus are not affected by meridional recirculation between 150°E and 120°W. It proves that the ventilation of the EUC is only a local process that always affects the same subregion of the EUC, that is, its upper periphery. In other words, two-thirds of the EUC transport (19 out of 28 Sv) in the eastern Pacific (120°W) originate from the western Pacific at 150°E (where they represent half of the flow). Only one-third of transport (9 Sv) corresponds to meridional supply of water associated with geostrophic convergence.

As discussed in section 2, the transport of the EUC exhibits a strong seasonal cycle, with an amplitude of the same magnitude as the annual-mean value. Though it contributes rather little to the annual-mean transport of the EUC, lateral circulation is able to modulate its mean seasonal cycle in a noticeable way. We find that over 90% of the EUC water found at 180° in January travels to 150°W, but the proportion drops to 60% for EUC water considered in June when the transport is the strongest: a large amount of the EUC mass is expelled by divergence. Equivalently, it is in June that the fraction of the water arriving at 180° from 150°E is the smallest (less than 70%): at that time of the year, geostrophy supplies the EUC with much water. On the contrary, this fraction is close to 95% in January (weak EUC transport and weak convergent phenomena). The direct mass transfer from the western Pacific to the eastern Pacific is in fact little affected by the seasonal modulation of the meridional circulation. The seasonal variability of the EUC transport is mostly induced by local recirculation phenomena, namely, variations of transport in the upper layers, which are the most sensitive to geostrophic convergence and Ekman divergence.

5. Sources and sinks of EUC water

a. Transports across the edges of the EUC

The analysis of the EUC mass budget in the central Pacific emphasizes the limited role of convergence in renewing EUC water. To determine the regions where water enters and leaves the EUC, we inject particles in the central Pacific and integrate their trajectories backward and forward in time until they leave the EUC. We consider that a given particle has left the EUC whenever the sign of its zonal velocity changes. We integrate particles from the EUC at 150°W and record the sign of their meridional velocity and their position at the exact moment when they leave the EUC. The sign of the meridional velocity conveniently defines whether a particle belongs to the southern or northern edge of the undercurrent.

Figure 7 displays the inflow and outflow locations of particles introduced at 150°W for sections corresponding to both meridional edges of the undercurrent. These figures are obtained by summing the elementary transports of particles, when they reach one edge, over small subregions (5° by 10 m) and by contouring the result. The spatial integration of the densities for both edges over half a zonal plane (east or west of 150°W, depending on the direction of integration) gives back the exact transport of the EUC at 150°W. The tick marks on the horizontal and vertical axes of Figs. 7a and 7b represent the proportion of ''northern-edge'' and ''southern-edge'' EUC transport respectively, after in-

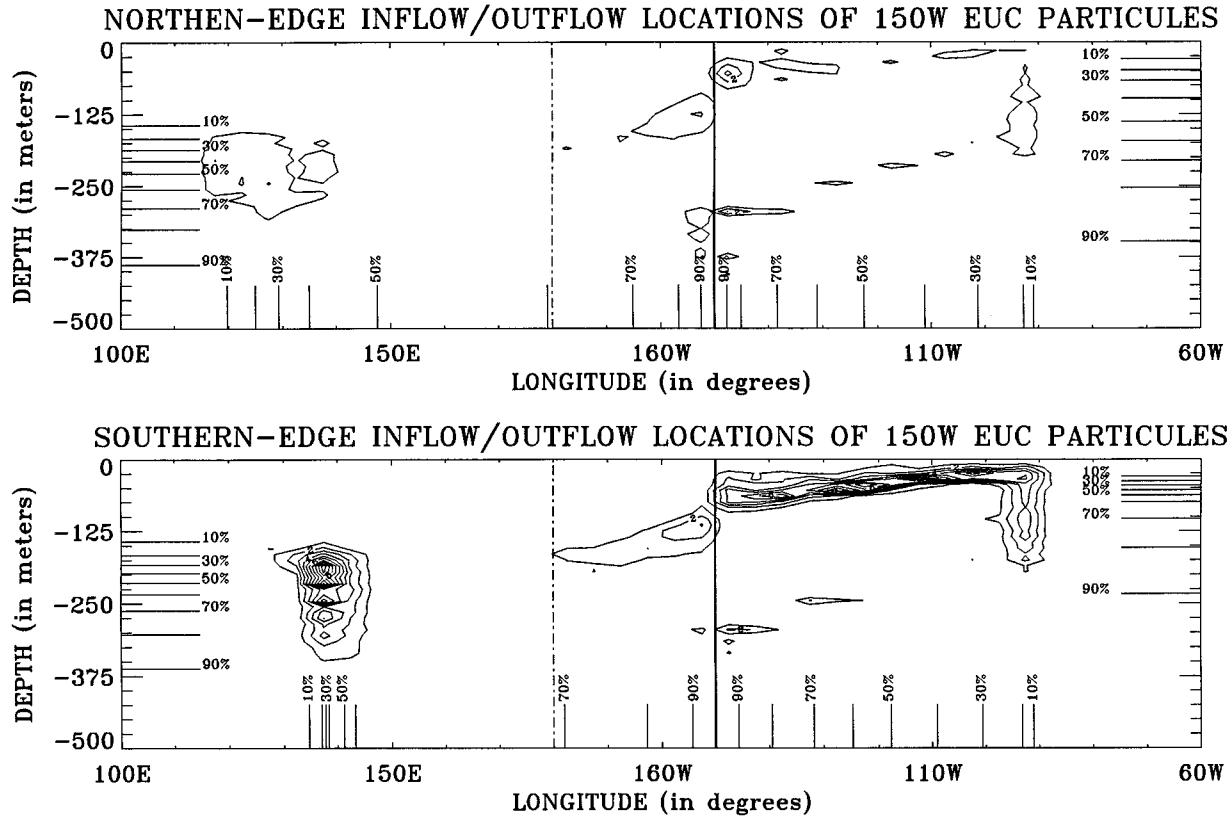

FIG. 7. Densities of transport of 150°W EUC water found on both meridional edges of the EUC. Left and right sides of the diagram correspond to sources and sinks of the EUC water respectively. The figures are obtained by locating the particles when they enter or leave the EUC (see text for details) and by contouring the result. (a) Section for the northern edge of the EUC. (b) Section for the southern edge of the EUC. The unit of density is arbitrary, but the contour interval is the same for both sections and both sides. Ticks on vertical and horizontal axes represent the percentage of ''southern edge related'' or ''northern edge related'' EUC transport after integrating the density from the surface to the bottom of the ocean, and from the coasts to 150°W. The interval between ticks is 10%.

tegrating the densities from the surface to the bottom of the ocean, or from the coasts to 150°W.

Continuous upward and poleward movements of water within the top layers of the EUC explain its ending. Just west of 90°W, some intense divergence is moreover caused by the sudden encounter of the EUC with the Galapagos Islands, deflecting it (see Lukas 1986) and forcing it to export most of its waters away from the equator, over its whole depth. We note here that the intensity of the EUC found in the model east of the Galapagos Islands is comparable to other estimates from direct measurements (Christensen 1971; Stevenson and Taft 1971; Lukas 1986). The shape of the area over which water exits poleward is inclined and fits the location of the uppermost layers of the EUC. A similar slope is found for the water entering the EUC by geostrophy, but at deeper levels (roughly 150 m) since this process is mostly active near the deepest levels of the SEC (see Fig. 4).

We consider now the windows in the western Pacific through which more than half of the EUC flow at 150°W is supplied. The mean latitude of the particles entering the EUC is 0.3°S on the southern window and 2.2°N on the northern window. There is, however, some variability around this mean value (the standard deviation is close to 1.5°) and particles on the southern edge may be located in the Northern Hemisphere. This occurs for instance close to Indonesia, where the coastline favors a northern position for the EUC. The main entry points are found within the western Pacific, north of New Guinea, with a possible extent toward Mindanao for the window on the northern edge. From observations of the dynamics in the western Pacific, mainly inferred from the Western Equatorial Pacific Ocean Circulation Study (WEPOCS) expeditions (Lindstrom et al. 1987), we can associate the narrow window on the southern edge with the New Guinea Undercurrent (NGUC) that flows northward along the coast from the Vitiaz Strait [for some useful references see for instance Fine et al. (1994)]. Part of the window on the northern edge is associated with the Mindanao Current that flows southward west of 130°E, as reported by Lukas et al. (1991).

Figure 8 displays with a heavy solid line how the EUC at 150°W is filled and emptied, by summing eastward and westward the transport associated with the particles found on the edge of the undercurrent at the

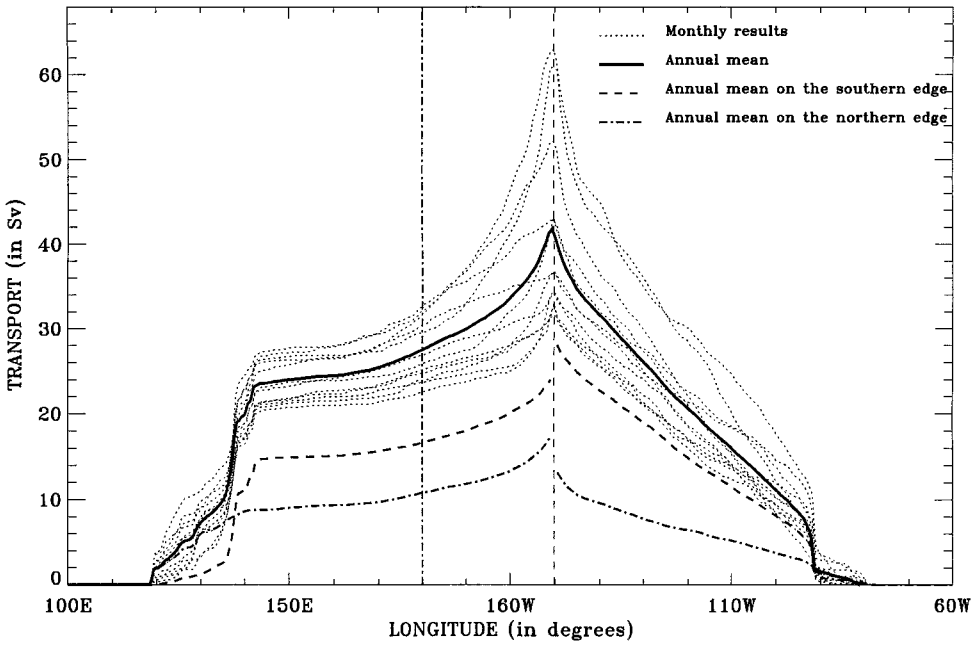

FIG. 8. Schematic diagram of the way the EUC at 150°W is filled (or emptied). On the left (or right) part of the figure, the solid line sums eastward (or westward) the transport associated with the particles found on the edge of the EUC at the end of their backward (or forward) time integration. Heavy dashed and mixed lines show equivalent computations except for the southern and northern edges separately. Light dotted lines give monthly results for the sum of the southern and northern edges.

end of their backward and forward integrations respectively. Both directions of calculation of course agree right at 150°W, by giving the annual-mean value of the transport over this section. Heavy dashed and mixed lines show equivalent computations except for the southern and northern edges separately. There is no need for these computations to match at 150°W since mass entering the EUC at one edge may leave it through the opposite one. Light dotted lines give results obtained for every month (for the sum of the southern and northern edges) and illustrate the seasonal variability associated with the EUC.

In the central Pacific (150°W) almost 60% of EUC is composed of water entering through its southern edge. The preferential source of EUC water is thus located southward. A sharp transition appears on all curves at 150°E and clearly discriminates two processes of inflow. The first one is found west of 150°E and corresponds to water supply from currents located close to the western boundary. The second one, east of 150°E and maximum near the initial section at 150°W, corresponds to some geostrophic convergence in the interior ocean. The relative weight of each process differs with the edge: Geostrophic convergence accounts for half of the supply on the northern edge, but only for less than 40% on the southern edge. The band of longitude over which western boundary inflow occurs is also different: The window is very small on the southern edge (close to 140°E), while it is wider on the northern edge (120°–140°E).

b. Transports across 15°N and 15°S

Figure 8 shows that the proportion of the water leaving the EUC by its southern edge (68%) is larger than the proportion of water entering the EUC by this same edge (58%). Though this is likely associated with the existence of interhemispheric exchange, we cannot be certain because both edges can be located in the same hemisphere. To diagnose such an exchange, we carry out extended Lagrangian integrations between 15°N and 15°S. These latitudes conveniently insulate the tropical oceanic circulation from the subtropical gyres, as recently evidenced in modeling experiments by Liu et al. (1994) and Lu and McCreary (1995). They also roughly correspond to the origins of both poleward western boundary currents, that is, the Kuroshio in the Northern Hemisphere and the East Australia Current in the Southern Hemisphere. We also define a new limit in the vertical at a deep level (3000 m) to detect possible connections of the EUC with the deep Pacific circulation. Trajectories of particles coming from or reaching the Indian Ocean are also stopped west of the Indonesian Throughflow. We integrate all particles from the EUC at 150°W, and we define as recirculating particles those coming back in the EUC at 150°W before reaching any other limit.

We calculated sections of ''density of transport'' at 15°S and 15°N, similar to those defined in section 5a, for each direction of integration. For the forward in-

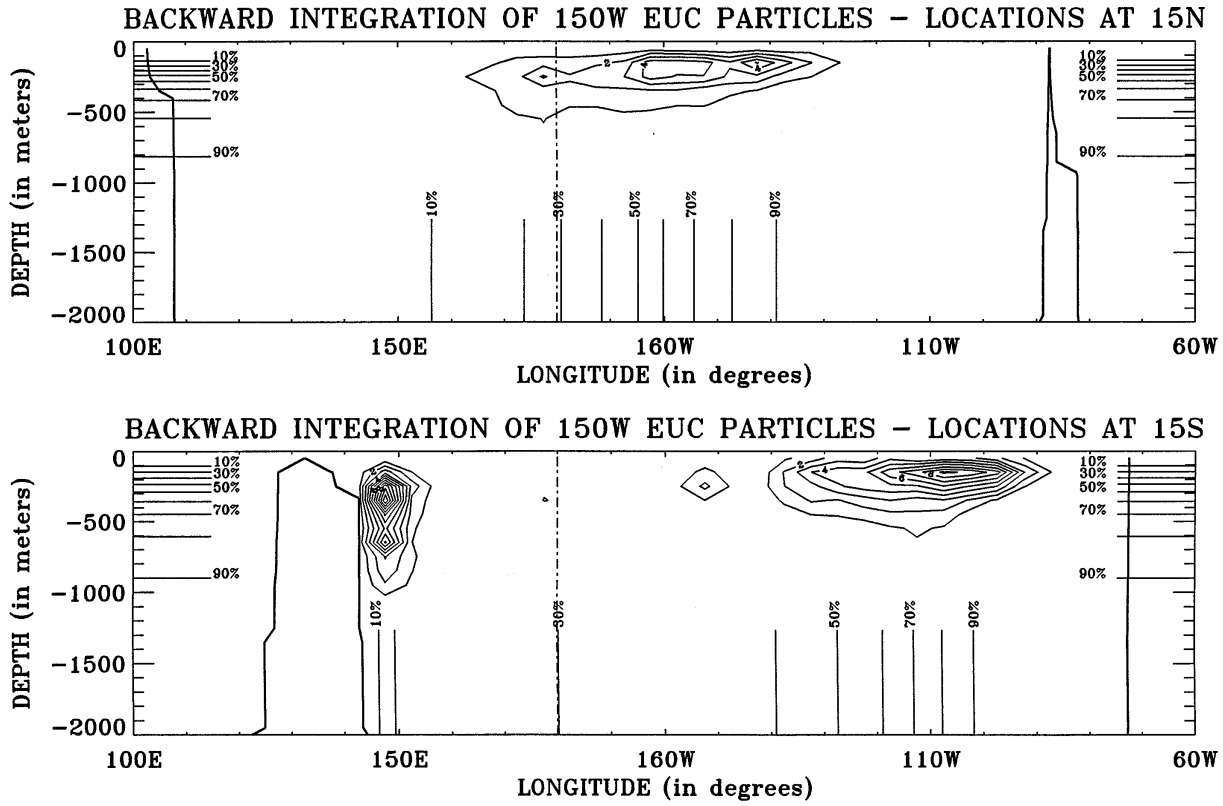

FIG. 9. Densities of transport of 150°W EUC water found, in backward integration, (a) at 15°N and (b) at 15°S. The unit of density is arbitrary but the contour interval is the same for both sections. Ticks on vertical and horizontal axes represent the percentage of the EUC transport explained after integrating the density eastward, and from the surface to the bottom of the ocean.

tegration (figure not shown), over 90% of nonrecirculating 150°W EUC water left the tropical domain within the upper 70 m of the ocean by upwelling at the equator before moving poleward. Over both sections, the distribution was spread over the whole domain in longitude, except near America where the surface currents essentially flow westward. Longer integrations performed until the particles reach 20°N or 20°S (not shown) revealed a progressive accumulation of mass on the western side of the basin. Indeed, both poleward western boundary currents (the Kuroshio and the East Australia Current) are supplied with water originating in the North Equatorial Current and SEC.

Figure 9 shows results for the backward integrations. More than 90% of EUC water is found within the top 1000 m (and almost all of it in the first 2000 m), but the domains in longitude differ. At 15°N the particles enter the tropical domain mostly between 160°E and 130°W and rather uniformly within and above the main thermocline. On the contrary, two distinct windows appear at 15°S. In addition to slow equatorward and westward movements in the ocean interior, distributed between 140° and 90°W and between depths −100 and −500 m, almost one-third of the total transport found at 15°S is concentrated in the immediate proximity of the western boundary, where the ocean GCM develops a subsurface northward boundary current, maximum at depth −300 m. Our approach cannot explain this asymmetry between 15°N and 15°S, but it is likely due to the intertropical convergence zone (ITCZ), as discussed by Lu and McCreary (1995).

Table 1 summarizes our main results by giving the fractions of 150°W EUC water found on the five boundaries and criteria we previously defined (15°S, 15°N, Indian Ocean, −3000 m, or EUC recirculation). The results are presented for both backward and forward integrations. For backward integrations, the table distinguishes flows that enter the EUC through either its northern or southern edge (as defined by the sign of the meridional velocity when associated particles join the EUC), west or east of 150°E.

First, we note that there is almost no connection between the EUC and the deep Pacific: only 0.5 Sv (out of 41.8 Sv) is found to originate from immersions deeper than 3000 m. Second, very little EUC water participates in the Indonesian Throughflow: only 1.8 Sv of its waters reach the Indian Ocean. In fact, most of EUC water (80%) leaves the tropical domain by crossing 15°N and 15°S.

The forward integrations indicate that the mass transported out of the domain across 15°N (17.3 Sv) is slightly higher than that transported to 15°S (15.7 Sv). These

TABLE 1. Mass balance of the EUC within the Tropics. All transports are expressed in Sverdrups. Backward and forward Lagrangian integrations are all performed from 150°W and they are stopped whenever a limit (15°S, 15°N, −3000 m, or Indian Ocean) is reached or whenever a given particulate recirculates within the EUC. The table distinguishes inflows and outflows on both northern and southern edges of the EUC, and, for backward integrations only, waters entering east and west of 150°E (hence the labels SW, SE, NW, and NE).

	Backward integration							Forward integration		
	Southern edge			Northern edge			Total backward	Southern edge	Northern edge	Total forward
	← 150°E	150°E →	Total	← 150°E	150°E →	Total				
Boundary at 15°N	1.1	0.9	2.0	6.4	3.3	9.7	11.7	10.3	7.0	17.3
Recirculation	0.3	3.3	3.6	0.2	2.8	3.0	6.6	4.1	2.7	6.8
Deep Pacific Ocean	0.1	0.1	0.2	0.2	0.1	0.3	0.5	0.1	0.1	0.2
Indian Ocean	0.2	0.0	0.2	0.3	0.1	0.4	0.6	1.5	0.3	1.8
Boundary at 15°S	13.3	4.8	18.1	1.8	2.5	4.3	22.4	12.4	3.3	15.7
Total	15.0 (SW)	9.1 (SE)	24.1	8.9 (NW)	8.8 (NE)	17.7	41.8	28.4	13.4	41.8

figures differ considerably from those obtained on the northern and southern edges of the EUC (13.4 and 28.4 Sv respectively), but they do not contradict them because some of the water that leaves the EUC southward, returns to the Northern Hemisphere within the SEC. The path followed by recirculating particles begins in a similar way, but they approach the equator at deeper levels within the SEC or they become captured by the North Equatorial Countercurrent that brings them back eastward, with a slow downwelling movement. Geostrophic convergence then allows them to join the EUC. This recirculation is consistent with the tropical cell defined by McCreary and Lu (1994).

The backward integrations demonstrate that the EUC is primarily sustained through its southern edge (24.1 Sv out of a total of 41.8 Sv, i.e., 58%), and we find that 66% of the extratropical EUC water comes from 15°S (22.4 Sv out of a total of 34.1 Sv). This proportion is again larger than the one diagnosed on the edges of the EUC because large eddies close to the Celebes Sea, such as the Halmahera eddy, can supply the EUC through its northern edge with water originating in the Southern Hemisphere (Fine et al. 1994). The coastal circulation in this region is, however, dominated by the Mindanao Current that flows southward and brings northern water to the EUC.

Our extended Lagrangian integrations indicate that the EUC contributes to a net exchange of water between both hemispheres. As shown in the backward integration portion of Table 1, the EUC consists mostly of water from the Southern Hemisphere: more than half of EUC water found at 150°W comes from 15°S (22.4 Sv) and less than a third from 15°N (11.7 Sv). We already noted that part of the southern water was, in fact, associated with recirculation within the EUC, but this only accounts for a few Sverdrups. On the other hand, the forward integration shows that EUC water at 150°W spreads rather uniformly over the Pacific Ocean surface and leaves the tropical domain at both meridional limits (15°S and 15°N) in a well-balanced way, 15.7 and 17.3 Sv respectively.

We estimate the net northward interhemispheric mass transfer associated with the EUC to be 5 to 6 Sv on an annual mean. In the absence of connections with the deep Pacific and the Indian Ocean, this value would match exactly the net outflow of 150°W EUC water at 15°N and the net inflow of 150°W EUC water at 15°S. In our analysis, both values differ slightly (5.6 and 6.7 Sv respectively) because there is some 150°W EUC water originating from and flowing to the Indian Ocean and the deep Pacific. However, in view of the poor connections of the EUC with these regions, we consider that the excess of 150°W EUC water at 15°N originates mostly from 15°S. This interhemispheric mass transfer that passes through the EUC roughly represents 15% of the EUC transport at 150°W, and it is of the same order as the water that recirculates within 15°S–15°N.

c. Main pathways

For visualizing paths of EUC water within the tropical domain, Fig. 10 displays backward trajectories of selected particles taken at 150°W for the annual-mean velocity field. The particles (labeled A to F) map most pathways suggested by Table 1. Particle A is typical of particles that recirculate in the EUC (almost 7 Sv), most of which enter the EUC east of 150°E (see Table 1). Note that the limit we chose at 15°S is likely to cut part of the recirculation path. By moving the southern limit to 20°S we estimated the total transport of water recirculating within the EUC as 10 Sv, that is, a fourth of the total transport at 150°W.

The origin of particles that belong to the EUC core at 150°W occurs in the northwestern region of the south subtropical gyre (see particle B). These results corroborate well those of Tsuchiya et al. (1989) who showed from hydrographic data (temperature, oxygen, and tritium) that the main origin of the EUC should be a west-

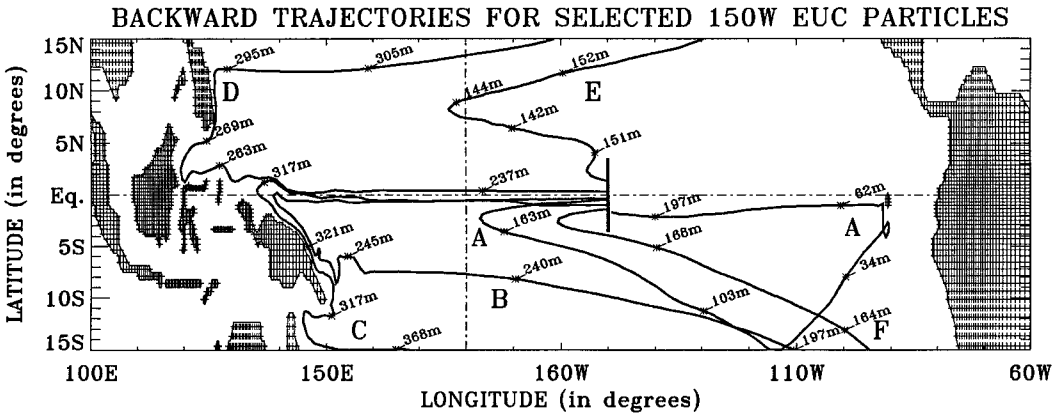

FIG. 10. Six selected backward trajectories (''A'' to ''F'') from the EUC at 150°W. Paths are typical of possible supplies of water to the EUC and are discussed in the text. Depths are given on trajectories.

ern boundary current flowing northwest along the coast of New Guinea (through the Strait of Vitiaz) and joining the equator between 135° and 145°E (depending on the season). They diagnose the origin of this current to be the south subtropical gyre. Our results confirm this hypothesis but also distinguish two separate paths (see also Fig. 9b). Particle B arrives in the tropical basin east of 120°W and crosses almost the whole Pacific at a depth of a few hundred meters (where SEC water converges equatorward) until it reaches the EUC, west of 150°E. Particle C enters the Tropics at deeper levels (down to 500 m) along the coast of East Australia within a narrow jet. There is no such distinction for Northern Hemisphere waters: All particles entering the Tropics west of 150°W follow a trajectory similar to that of particle D, first flowing within the North Equatorial Current, then the Mindanao Current.

Particles entering the Tropics within the eastern Pacific (e.g., east of 150°W at 15°N) do not join the western boundary current system: They reach the equator in a more gentle way (as particles E and F), being mostly sensitive to geostrophic convergence. The contrast we have at 15°N (i.e., a different behavior for particles entering the Tropics west or east of 150°W) agrees with Liu et al.'s (1994) results. Note that we have convergence within the ocean interior, from the Tropics to the equator, for both hemispheres (particles E and F), but the transport from 15°N is smaller than from 15°S (see Table 1). The path followed by particle E does not exist in Lu and McCreary's (1995) second-layer velocity field because of a potential-vorticity barrier produced by the ITCZ. It is likely that this constraint is weakened in our model (due to vertical mixing and high resolution of the GCM in the upper 200 m), allowing flow from the Northern Hemisphere to the equator in the interior ocean.

Initial locations of particles A to F on a meridional section of the EUC are given in Fig. 11. The origins for particles distributed every twelfth degree × 9 m are indicated with a specific symbol (see legend). The Lagrangian diagnostics were smooth enough to let us divide this EUC section into four subregions, each of them associated with one possible EUC origin as listed in Table 1. Subregion SW (or NW) represents EUC water originating from the southern (or northern) EUC edge within the western boundary current system. Such water flows principally from 15°S and 15°N, and it corresponds to the deep and core-related EUC layers. Subregion SE is associated with southern-edge-related converging water (entering the EUC east of 150°E). It includes extratropical particles (such as F) and recirculating water (such as A). An equivalent domain is found for the northern edge (subregion NE): Particle E is one example of water originating in the Northern Hemisphere.

The equatorial divergence is active all over the eastern Pacific Ocean, even east and southeast of the Galapagos Islands. The last waters of the EUC to be upwelled and exported poleward are located near the coast of America. Since most of the upwelled water belong to the surface layers of the Pacific, they move rapidly away from the equator, reaching 15°S or 15°N in a few years. At that time, a fraction of the EUC is still located at the equator, near the coast. The particles within the southeastern part of this group originate in the lower part of the EUC core at 150°W. Integrating the trajectories a few more years shows that these particles finally leave the equator and merge with the surface general circulation of the Pacific Ocean.

6. Conclusions

The Pacific Equatorial Undercurrent mostly owes its existence to the trade winds that establish a zonal pressure gradient throughout the Tropics. Along the equator, this gradient draws water from the western boundary currents that originate in the north and south subtropical gyres. In the rest of the Tropics, it causes geostrophic convergence that can also contribute to the EUC. In this study we used three-dimensional monthly velocity fields

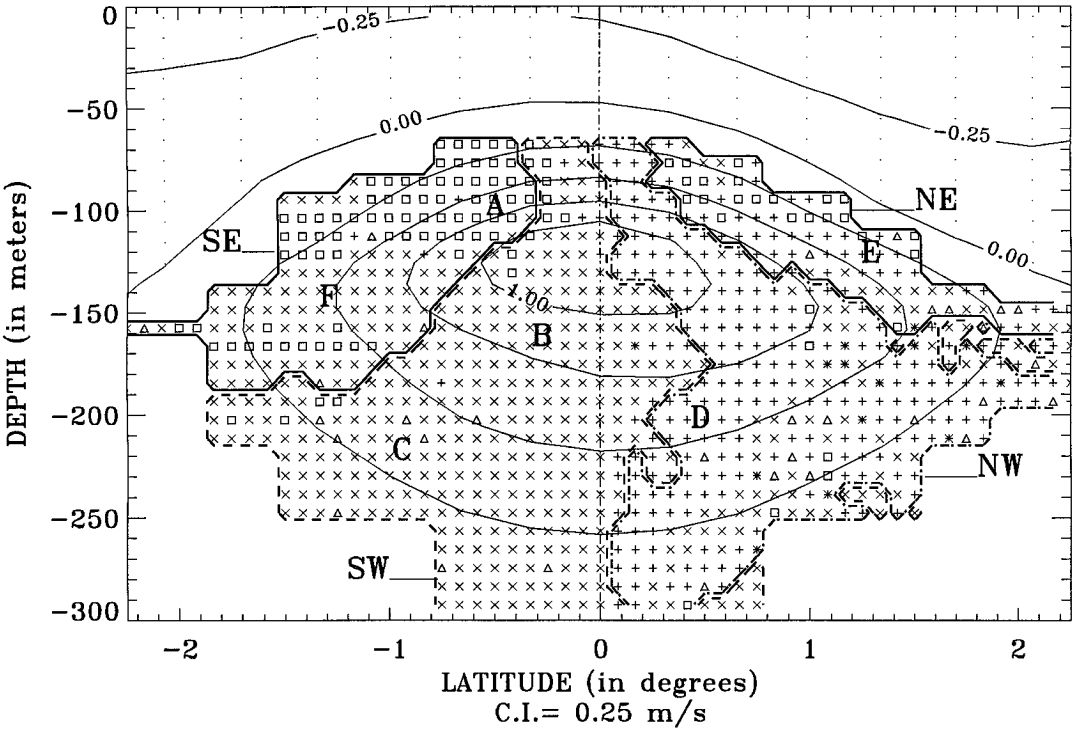

FIG. 11. Origins of EUC water found at 150°W: symbols are ''plus'' for 15°N, ''cross'' for 15°S, ''triangle'' for depth −3000 m, ''star'' for the Indian Ocean, and ''square'' for recirculating EUC particles. Initial positions of particles A to F, as discussed in the text, are also given. Subregions SW, NW, SE, and NE as defined in Table 1 are delimited.

from an ocean GCM to study the mass balance within the EUC. We particularly use some Lagrangian diagnostics to evaluate accurately various mass transfers between several sections of the EUC, and between the EUC domain and the Tropics. Such diagnostics consist largely of the description and study of the EUC with a very large number of individual particles, each associated with a given elementary transport and each tracked within the tropical domain.

First diagnostics are simple Eulerian descriptions. They deal with the EUC domain and aim at depicting the dynamics of the EUC. A clear asymmetry is shown between the western and eastern Pacific: though converging water is mostly found in the center of the basin (both north and south of the EUC), divergent water is particularly escaping the EUC northward in the western domain and southward in the eastern domain. The decomposition of the meridional fluxes in divergent Ekman and convergent geostrophic transports helps us to link these asymmetries to the annual-mean structure of the wind stress over the area. The specific role of the geostrophic convergence in supplying water to the EUC is addressed by means of Lagrangian integrations. We show that such waters only ventilate the upper layers of the EUC and only belong temporarily to it, but they explain a large part of the seasonal variability of the EUC transport in the model. Finally, and as shown by Pedlosky (1988) but with an ideal fluid model, the ending of the EUC is mostly a continuous process active in the central and eastern Pacific.

Since the EUC really resembles a tongue of water that flows eastward from the western Pacific to the coast of South America, we perform Lagrangian integrations to evaluate the way the EUC is filled and emptied over the whole basin. Major paths for entering waters within the EUC are illustrated and quantified, as well as the amount of water that recirculates within the EUC before leaving the tropical domain (more than 15% of 41.8 Sv at 150°W). We are able to evaluate the rate at which the EUC exports its waters upward and then poleward, and to visualize the main exit windows for EUC water initially considered at 150°W. The fraction of EUC water that diverges southward is almost 70% in the model. This value is compatible with available qualitative descriptions of the termination of the EUC as reviewed and studied by Lukas (1986): the Galapagos Islands considerably disrupt the EUC in the model by hastening its termination. Most of the EUC water is injected in the surface layers (North Equatorial Current and SEC) with only little continuing its way to and along the coast of South America.

Our study did not aim at investigating thoroughly the connections between the subtropical and equatorial ocean circulations, as specifically addressed by McCreary and Lu (1994), Liu et al. (1994), and Lu and McCreary(1995), yet we find that the EUC actively

takes part in interhemispheric exchange of water. We are able to estimate precisely the various ways of feeding it at the western boundary. As in Liu et al. (1994) for an idealized rectangular basin, we can distinguish two ways equatorial regions and the Tropics are linked through the undercurrent, namely, through the western boundary currents and the oceanic interior, from the southern and northern Tropics.

Further studies will address a larger spectrum of the temporal variability of the tropical ocean circulation. Indeed, the EUC flow is likely to interfere with the whole dynamics of the Pacific Ocean in anomalous situations linked to ENSO variability, as suggested by its vanishing during warm episodes. Moreover, the timescales associated with the recirculation of EUC water in the tropical Pacific, and with the supply of EUC water by the subtropical thermocline, are found in this study to be on the order of a few years. This suggests that EUC dynamics needs to be analyzed in close connection with ENSO dynamics, preferably with outputs from a coupled atmospheric and ocean model. Smaller timescales need to be investigated too. Westward propagating tropical instability waves linked to sharp fronts in the equatorial Pacific, with a period of 15 to 30 days, are likely to affect the structure of the EUC. Since ocean general circulation models now show some success in addressing these phenomena, so long as an adequate atmospheric forcing is provided, they could help in diagnosing their impact on the large-scale dynamics. Finally, the Lagrangian diagnostics we developed for the present study could be applied easily to other well spatially defined ocean currents, not necessarily flowing in the tropical Pacific.

Acknowledgments. We thank Pascale Delecluse and Gurvan Madec for many useful discussions during this study. We are also indebted to Christophe Maes for providing us the results of his simulation run with OPA. We thank Anthony Weaver, Kevin Speer, and Sabrina Speich for their assistance in the correction of the manuscript. It is a pleasure to acknowledge comments and suggestions by the editor, Julian P. McCreary, which influenced the revisions and considerably improved the legibility of the paper. Part of the study was initiated during the stage de DEA of SR at LODYC. Support for this study has been provided by the Centre National de la Recherche Scientifique (CNRS). Lagrangian computations were performed on the Cray C94 of the Institut du Développement et des Ressources en Informatique Scientifique (IDRIS) and analyzed with the computational resources available at LODYC.

APPENDIX

Analytical Formulation of the Three-Dimensional Streamfunction on a C Grid

Usual ways to compute trajectories from GCM outputs involve first the interpolation of the three-dimensional velocity at the location of a given particle, then the advection of this particle in the direction of the current. Such methods require accurate interpolation and advection schemes to minimize possible cumulative errors in the computation of the trajectories. In the present study, we take advantage of the ''C'' grid (Arakawa 1972) used for discretizations in the OPA model to compute analytically trajectories from model outputs. The algorithm calculates true trajectories for a given stationary velocity field through the exact computation of three-dimensional streamlines. Under the assumption of stationarity, such streamlines indeed represent trajectories of particles advected by the given velocity field.

The three components of the velocity are known over the six faces of each cell. The nondivergence of the velocity field then ensures continuous trajectories within this cell. We develop here some equations with the tensorial formalism used in the OPA model (Marti et al. 1992), which allows a more general approach than a simple Cartesian view, with for instance the description of a distorted grid over the sphere. Using the same notations as Marti et al. (1992), the divergence of the three-dimensional velocity field $\mathbf{V} = (U, V, W)$ is expressed as

$$\Delta\mathbf{V} = \frac{1}{b}[\partial_i(e_2e_3U) + \partial_j(e_1e_3V) + \partial_k(e_1e_2W)], \tag{A.1}$$

where $n = i, j,$ or k refers to the grid index for the three axes; ∂_n refers to the corresponding finite difference; e_1, e_2, and e_3 are the scale factors (in the three directions) computed at each velocity grid point; and b is the product $e_1e_2e_3$ computed at the center of a given cell (''temperature'' grid point). For any choice of the grid, the nondivergence of the flow now simply writes as

$$\partial_iF + \partial_jG + \partial_kH = 0, \tag{A.2}$$

where F, G, and H designate the transports in the three directions, with $F = e_2e_3U$, etc.

We assume now that the three components of the transport vary linearly between two opposite faces of one individual cell. This hypothesis respects the local three-dimensional nondivergence of the flow. It means that, within a given cell, F depends linearly on i, G depends linearly on j, and H depends linearly on k, where i, j, and k are considered as fractional within the cell (i.e., as noninteger). In the cell extending from $i = 0$ to $i = 1$, one can write for instance for F

$$F(r) = F_0 + r\Delta F, \tag{A.3}$$

with $r \in [0, 1]$ and $F(0) = F_0$, and where ΔF stands for $F(1) - F(0)$. One can also write the equation linking position and velocity, namely $dx/dt = U$, for the transport

$$\frac{dr}{ds} = F, \tag{A.4}$$

with $s = (e_1e_2e_3)^{-1}t$ and $x = e_1r$. With some adequate initial conditions, for example, $r = 0$ for $s = 0$, one can combine (A.3) and (A.4) and find the time dependency of r within the considered cell

$$r = \frac{F_0}{\Delta F}[\exp(\Delta F s) - 1]. \tag{A.5a}$$

If $\Delta F = 0$, only the limit of (A.5a) for $\Delta F \to 0$ is to be considered

$$r = F_0 s. \tag{A.5b}$$

Similar relationships are of course obtained along both other directions. Since these expressions only apply in one individual cell, one also has to determine the time when a given particle switches to another cell, or equivalently the time when r is equal to its exit value (here $r = 1$). Time dependency is obtained from a different writing of (A.4):

$$ds = \frac{dr}{F}. \tag{A.6}$$

Using (A.3), one obtains the following expression for ds:

$$ds = \frac{dF}{F\Delta F}. \tag{A.7}$$

A crossing time in the zonal direction can only be obtained if $F(1)$ and $F(0)$ have the same sign, and this implies $F \neq 0$ in the cell. If this condition is not verified for F, the three-dimensional nondivergence of the velocity field ensures that at least one other direction satisfies it. One can assume that this condition is checked in the zonal direction. The pseudo time s is then related to the transport F by

$$s = \frac{1}{\Delta F} \ln\left(\frac{F}{F_0}\right). \tag{A.8}$$

The crossing time in this direction corresponds to the moment when the transport reaches the exit face value, $F(1)$:

$$\Delta s = \frac{1}{\Delta F} \ln\left(\frac{F_1}{F_0}\right), \tag{A.9a}$$

or, if $\Delta F = 0$, its limit when $\Delta F \to 0$:

$$\Delta s = \frac{1}{F_0}. \tag{A.9b}$$

As previously mentioned, at least one of the three crossing times is to be defined through such a formulation. The shortest one defines the traveling time in the considered cell. Thus, if the particle first attains the zonal extremity of the cell, its positions on the meridional and vertical axes are deduced from the equations of the trajectories using $s = \Delta s$. Computations are done for the next cell, with a starting point equal to the exit point of the previous one, and the ''age'' of the particle is regularly updated summing the expressions (A.9) obtained for Δs.

This method for computing trajectories is both fast and accurate: it only calculates positions on the edge of individual grid cells, and it fully respects the local three-dimensional nondivergence of the flow. The method is flexible too, and backward integrations can be performed to track the origin of a given current. Quantitative results are obtained by increasing considerably the number of particles. Due to water incompressibility, one given particle with an infinitesimal section is to conserve its infinitesimal mass along its trajectory. As a current can be entirely determined by the particles that compose it, with well-defined characteristics (position, velocity, and other scalars), the transport of a given water mass can be calculated from its own particles and their associated infinitesimal transport.

The best positioning of the particles (over initial sections) is the one that gives the highest accuracy in the computation of the transports associated with the circulation, for a reasonable number of initial positions. A measurement of the accuracy is the difference between ''section to section'' transports computed for a stationary velocity field with both forward and backward integrations, as both transports are virtually equal. ''Constant number of particles by grid cell'' and ''spatially homogeneous distributions'' are not satisfactory because they may use too few (many) particles to describe regions of weak (slow) currents. A sophisticated approach would distribute particles so that they have the same transport, thus grouping them in regions where the velocity is the highest. The algorithm is not easy to implement, but one can be satisfied with a simpler formulation where the area of each individual grid cell (with a given transport T_i) is divided into N_i^2 subregions, with N_i satisfying

$$\frac{T_i}{N_i^2} \leq T_0, \tag{A.10}$$

where T_0 is a prescribed maximum transport for any given particle. The total number of particles is the sum of the N_i, and a homogeneous distribution is adopted within each grid cell. This is the distribution we use to obtain all our quantitative results.

REFERENCES

Arakawa, A., 1972: Design of the UCLA general circulation model. Numerical simulation of weather and climate. Tech. Rep. 7, Dept. of Meteorology, University of California, Los Angeles, 116 pp.

Blanke, B., and P. Delecluse, 1993: Variability of the tropical Atlantic Ocean simulated by a general circulation model with two different mixed-layer physics. *J. Phys. Oceanogr.*, **23,** 1363–1388.

Boulanger, J.-P., C. Maes, P. Delecluse, and C. Lévy, 1996: Equatorial waves in an OGCM. *Mon. Wea. Rev.*, in press.

Chiswell, S. M., K. A. Donohue, and M. Wimbush, 1995: Variability in the central equatorial Pacific, 1985–1989. *J. Geophys. Res.*, **100,** 15 849–15 863.

Christensen, N., Jr., 1971: Observations of the Cromwell Current near the Galapagos Islands. *Deep-Sea Res.,* **18,** 27–33.

Delcroix, T., G. Eldin, M.-H. Radenac, J. Toole, and E. Firing, 1992: Variation of the western equatorial Pacific Ocean, 1986–1988. *J. Geophys. Res.,* **97,** 5423–5445.

Delecluse, P., G. Madec, M. Imbard, and C. Lévy, 1993: OPA version 7 Ocean General Circulation Model—Reference Manual. Rapport Interne LODYC 93/05, 111 pp. [Available from LODYC, Université Pierre et Marie Curie, Paris.]

——, J. Servain, C. Lévy, K. Arpe, and L. Bengtsson, 1994: On the connection between the 1984 Atlantic warm event and the 1982–1983 ENSO. *Tellus,* **46A,** 448–464.

Esbensen, S. K., and V. Kushnir, 1981: The heat budget of the global ocean: An atlas based on estimates from marine surface observations. Climatic Research Institution Rep. 29, 27 pp.

Fine, R. A., R. Lukas, F. M. Bingham, M. J. Warner, and R. H. Gammon, 1994: The western equatorial Pacific: A water mass crossroads. *J. Geophys. Res.,* **99,** 25 063–25 080.

Firing, E., R. Lukas, J. Sadler, and K. Wyrtki, 1983: Equatorial Undercurrent disappears during 1982–1983 El Niño. *Science,* **222,** p. 1121.

Hellerman, S., and M. Rosenstein, 1983: Normal monthly wind stress over the world ocean with error estimates. *J. Phys. Oceanogr.,* **13,** 1093–1104.

Levitus, S., 1982: *Climatological Atlas of the World Ocean.* NOAA Prof. Paper No. 13, U.S. Govt. Printing Office, 173 pp.

Lindstrom, E., R. Lukas, R. Fine, E. Firing, S. Godfrey, G. Meyers, and M. Tsuchiya, 1987: The Western Equatorial Pacific Ocean Circulation Study. *Nature,* **330,** 533–537.

Liu, Z., 1994: A simple model of the mass exchange between the subtropical and tropical ocean. *J. Phys. Oceanogr.,* **24,** 1153–1165.

——, S. G. H. Philander, and R. C. Pacanowski, 1994: A GCM study of tropical–subtropical upper-ocean water exchange. *J. Phys. Oceanogr.,* **24,** 2606–2623.

Lu, P., and J. P. McCreary Jr., 1995: Influence of the ITCZ on the flow of thermocline water from the subtropical to the equatorial Pacific Ocean. *J. Phys. Oceanogr.,* **25,** 3076–3088.

Lukas, R., 1986: The termination of the Equatorial Undercurrent in the eastern Pacific. *Progress in Oceanography,* Vol. 16, Pergammon, 63–90.

——, E. Firing, P. Hacker, P. L. Richardson, C. A. Collins, R. Fine, and R. Gammon, 1991: Observations of the Mindanao Current during the Western Equatorial Pacific Ocean Circulation Study. *J. Geophys. Res.,* **96,** 7089–7104.

Maes, C., G. Madec, and P. Delecluse, 1997: Sensitivity of an equatorial Pacific OGCM to lateral diffusion. *Mon. Wea. Rev.,* **125,** 958–971.

Marti, O., G. Madec, and P. Delecluse, 1992: Comment on ''Net diffusivity in ocean general circulation models with nonuniform grids'' by F. L. Yin and I. Y. Fung. *J. Geophys. Res.,* **97,** 12 763–12 766.

McCreary, J. P., Jr., and P. Lu, 1994: Interaction between the subtropical and equatorial ocean circulations: The subtropical cell. *J. Phys. Oceanogr.,* **24,** 466–497.

Pedlosky, J., 1987: An inertial theory of the Equatorial Undercurrent. *J. Phys. Oceanogr.,* **17,** 1978–1985.

——, 1988: Entrainment and the termination of the Equatorial Undercurrent. *J. Phys. Oceanogr.,* **18,** 880–886.

——, 1991: The link between western boundary currents and equatorial undercurrents. *J. Phys. Oceanogr.,* **21,** 1553–1558.

Picaut, J., and R. Tournier, 1991: Monitoring the 1979–1985 equatorial Pacific current transports with expandable bathythermograph data. *J. Geophys. Res.,* **96,** 3263–3277.

Speich, S., 1992: Etude du forçage de la circulation océanique par les détroits: Cas de la Mer d'Alboran. Thèse de 3ème cycle, Université Pierre et Marie Curie, 245 pp.

Stevenson, M. R., and B. A. Taft, 1970: New evidence of the Equatorial Undercurrent east of the Galapagos Islands. *J. Mar. Res.,* **29,** 103–115.

Tsuchiya, M., 1981: The origin of the Pacific equatorial 13°C water. *J. Phys. Oceanogr.,* **11,** 794–812.

——, R. Lukas, R. A. Fine, E. Firing, and E. Lindstrom, 1989: Source waters of the Pacific Equatorial Undercurrent. *Progress in Oceanography,* Vol. 23, Pergammon, 101–147.

Wacongne, S., 1989: Dynamical regimes of a fully nonlinear stratified model of the Atlantic Equatorial Undercurrent. *J. Geophys. Res.,* **94,** 4801–4815.

——, 1990: On the difference in strength between Atlantic and Pacific undercurrents. *J. Phys. Oceanogr.,* **20,** 792–799.